Marine Chemistry 243 (2022) 104134

Contents lists available at ScienceDirect

Marine Chemistry

journal homepage: www.elsevier.com/locate/marchem

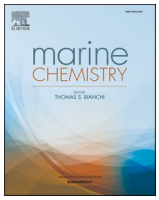

The role of pH up-regulation in response to nutrient-enriched, low-pH groundwater discharge

Nancy G. Prouty [a,*], Marlene Wall [b], Jan Fietzke [b], Olivia M. Cheriton [a], Eleni Anagnostou [b], Brian L. Phillips [c], Adina Paytan [d]

[a] U.S. Geological Survey, Coastal and Marine Geology, Pacific Coastal and Marine Science Center, Santa Cruz, CA 95060, United States of America
[b] GEOMAR Helmholtz Centre for Ocean Research Kiel, Wischhofstr. 1-3, 24148 Kiel, Germany
[c] Department of Geosciences, Stony Brook University, Stony Brook, NY 11794-2100, United States of America
[d] Institute of Marine Sciences, University of California at Santa Cruz, Santa Cruz, CA 95064, United States of America

ARTICLE INFO

Keywords:
Groundwater pollution
Coral reefs
Sewage effluent
Acidification
Eutrophication

ABSTRACT

Coral reefs and their ecosystems are threatened by both global stressors, including increasing sea-surface temperatures and ocean acidification (OA), and local stressors such as land-based sources of pollution that can magnify the effects of OA. Corals can physiologically control the chemistry of their internal calcifying fluids (CF) and can thereby regulate their calcification process. Specifically, increasing aragonite saturation state in the CF (Ω_{CF}) may allow corals to calcify even under external low saturation conditions. Questions remain regarding the physiological processes that govern the CF chemistry and how they change in response to multiple stressors. To address this knowledge gap, the boron $\delta^{11}B$ and B/Ca were analyzed in tropical corals, *Porites lobata,* collected at submarine groundwater seeps impacted by the release of treated wastewater in west Maui, Hawai'i, to document the interactions between high nutrient / low pH seep water on CF carbonate chemistry. Results show substantial up-regulation of pH and dissolved inorganic carbon (DIC) with respect to seawater in *P. lobata* corals collected from within the wastewater impacted area at Kahekili Beach Park compared to the control site at Olowalu Beach. The Ω_{CF} was 9 to 10 times higher than ambient seawater Ω, and 13 to 26% higher than in corals from the control site and from values previously observed in tropical *Porites* spp. corals. Such elevated up-regulation suggests that corals exposed to nutrient-enriched, low pH effluent sustain CF supersaturated with respect to aragonite, possibly as an internal coping mechanism to combat multiple stressors from land-based sources of pollution. This elevated up-regulation has implications to coral vulnerability to future climate- and ocean-change.

1. Introduction

Global climate change, including increasing sea-surface temperatures (SSTs) and ocean acidification (OA), together with local stressors that impact water quality, such as increased sedimentation or eutrophication, synergistically threaten coral reef health (e.g., Crain et al., 2008). Given the diverse ecosystems services provided by coral reefs (e.g., Woodhead et al., 2019), including the protective services created by reef structure (Storlazzi et al., 2019), there is growing scientific interest in understanding coral reef resilience. Specifically, global surface OA triggered by the rise in atmospheric carbon dioxide fundamentally alters seawater chemistry, decreasing pH and reducing the concentration of carbonate ions ($[CO_3^{2-}]$), thereby negatively impacting reef building corals and their ability to maintain high skeletal growth and/or density (Hennige et al., 2015; Kamenos and Hennige, 2018; Langdon and Atkinson, 2005; Ries et al., 2009). The ability of corals to physiologically mediate the chemistry of their calcifying fluid (CF) indicates that corals can control their calcification process, possibly allowing them to calcify under a larger range of conditions (e.g., McCulloch et al., 2012a; McCulloch et al., 2017; Wall et al., 2016). However, the impact of various environmental compounding stressors on this ability has not been thoroughly studied in the field under environmentally relevant and authentic, naturally variable conditions.

Biological regulation of the calcifying medium within the extracellular sites of calcification allows corals to modulate the carbonate chemistry at the site of calcification to facilitate calcification (Al-Horani et al., 2003a; Venn et al., 2011). This process creates a pH gradient between the CF and the surrounding seawater, where protons are

* Corresponding author.
E-mail address: nprouty@usgs.gov (N.G. Prouty).

https://doi.org/10.1016/j.marchem.2022.104134
Received 10 February 2022; Received in revised form 20 May 2022; Accepted 22 May 2022
Available online 29 May 2022

pumped out of the calicoblastic space between the coral tissue and skeleton to maintain high pH within the CF (pH_{CF}) (Al-Horani et al., 2003b; Venn et al., 2011). Removal of protons from the calcification site via Ca^{2+}-ATPase activity has been hypothesized in both shallow (zooxanthellae-bearing) corals (Wall et al., 2016), temperate corals (Trotter et al., 2011), and cold-water (azooxanthellate) corals (McCulloch et al., 2012b; Rollion-Bard et al., 2011). However, the magnitude of pH increase in the CF relative to ambient seawater (ΔpH the difference between the pH in the CF and that of seawater) as well as the absolute pH_{CF} has shown to be larger in azooxanthellate cold-water corals (McCulloch et al., 2018). To date CF pH has been measured directly by confocal microscopy and microelectrodes confirming an upregulation of pH and dissolved inorganic carbon (DIC) within the CF (e.g., Al-Horani et al., 2003b; Sevilgen et al., 2019; Venn et al., 2013) and thus the ability of $\delta^{11}B$ and B/Ca to indirectly constrain the CF carbonate system (Allison, 2017; DeCarlo et al., 2018; Holcomb et al., 2016; Mavromatis et al., 2015; McCulloch et al., 2017). Measuring both $\delta^{11}B$ and B/Ca allows for calculating pH_{CF} and estimating carbonate ion $[CO_3^{2-}]_{CF}$, respectively (Hemming and Hanson, 1992; Klochko et al., 2006), holding promise in constraining the full carbonate system within the CF over time. This

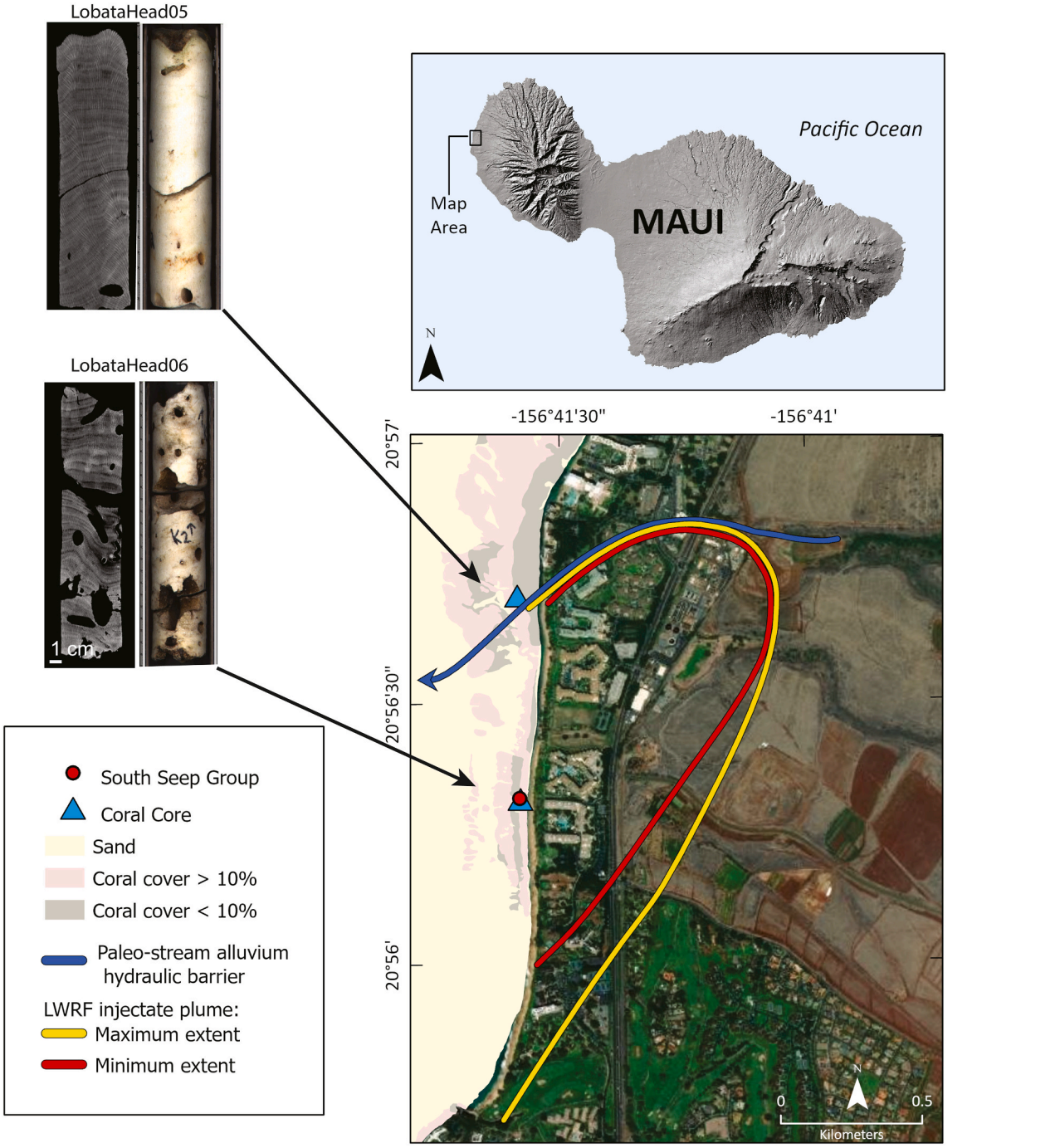

Fig. 1. Location map of the island of Maui, Hawai'i, USA, and the study area at Kahekili Beach Park along west Maui showing coral coring locations, the South Seep Group (SSG; red circle), superimposed on distribution of percent coral cover versus sand. Computerized tomography (CT) images and respective photographs of coral cores collected at the SSG and to the north, approximately 780 m north of the SSG. Spatial extents of the Lahaina Wastewater Reclamation Facility (LWRF) injectate plume (red and yellow) and inferred subsurface paleo-stream alluvium hydraulic barrier (blue) also shown. Modified from Hunt Jr. and Rosa (2009) and Prouty et al. (2017a). (For interpretation of the references to colour in this figure legend, the reader is referred to the web version of this article.)

calculation assumes that only borate is incorporated into the carbonate skeleton during coral calcification and requires auxiliary data such as temperature and salinity, and the B distribution coefficient. Studies using coral skeletal B systematics have shed some light on coral resilience to OA and potential acclimatization of corals to naturally occurring low-pH environments (McCulloch et al., 2012a; Wall et al., 2019a; Wall et al., 2019b). However, questions remain regarding the ability of corals to effectively regulate the CF chemistry when faced with the effects of both low-pH and elevated nutrient conditions.

Submarine groundwater discharge (SGD) has been documented at the shallow reef off Kahekili Beach Park in Kā'anapali, west Maui. The discharging groundwater is nutrient rich and has lower than ambient seawater pH exposing corals in the vicinity of these SGD seeps to these combined stressors. The SGD contains treated effluent water, which is injected to the groundwater at the nearby Lahaina Wastewater Reclamation Facility (LWRF, in operation since 1976) (Glenn et al., 2013; Murray et al., 2019; Swarzenski et al., 2017). Reef health and coral cover have been declining along the shallow coral reef at Kahekili Beach Park (Ross et al., 2012; Wiltse, 1996) with documented re-occurrence of seasonal (winter) macro-algal blooms (Smith et al., 2005) and shifts in benthic cover from abundant coral to turf- or macro-algae (Cochran et al., 2014). Following a large bleaching event in 2015, the coral cover declined further, with *P. lobata* exhibiting the largest absolute decline in percent cover (McCarthy, UCSD, written commun, 2021). Bioerosion rates of *Porites* spp. corals growing close to the SGD seeps are also high and corals showed lower net calcification rates (Prouty et al., 2017a). Secondary effects of eutrophication have also been reported at Kahekili Beach Park such as a shift from net community production and calcification to net respiration and carbonate dissolution (Prouty et al., 2018). Here we use coupled $\delta^{11}B$ and B/Ca measurements to investigate the effect of the combined low pH and elevated nutrients on the CF carbonate chemistry of the coral *P. lobata*, document ΔpH, and evaluate the environmental conditions influencing CF carbonate chemistry.

2. Methods

2.1. Study site and coral collection

Coral cores from the shallow reef at Kahekili Beach Park in Kā'anapali, west Maui, Hawai'i, were collected in July 2013 as described in Prouty et al. (2017a) (Fig. 1). In brief, two coral cores from scleractinian *P. lobata* were drilled offshore from the Kahekili Beach Park, approximately 0.5 km southwest of the LWRF, and where previous work has located clusters of brackish SGD seeps influenced by the LWRF injectate plume (Glenn et al., 2013; Swarzenski et al., 2017) and contaminants including pharmaceuticals and flame retardants (Campbell et al., 2017). A single core was collected from a coral head (LobataHead06) within the active south seep cluster (referred to as the South Seep Group, SSG), 23 m offshore in a water depth of less than 1 m. At this site, the salinity, temperature, and pH vary as a function of SGD flux (Swarzenski et al., 2017). According to a 2012–2013 survey using a piezometer inserted into a seep, SGD salinity varied between 3.8 and 22, pH varied between 7.2 and 7.9, and water temperatures were > 28 °C (Glenn et al., 2013). Similarly, based on a survey using Solinst CTD Divers deployed on the seafloor at the SSG during a 6-d sampling period in March 2016 (Prouty et al., 2018), bottom water salinity varied between 10.6 and 36.7 and temperature ranged from 23.2 to 26.4 °C, whereas salinity on the reef flat did not drop below 30 (Prouty et al., 2017b). The SGD at this site is characterized by elevated nitrogen and nitrogen isotope ($\delta^{15}N$) of nitrate (Dailer et al., 2010; Hunt Jr. and Rosa, 2009). Nitrate concentrations of the SGD were as high as 117 μmol L^{-1} with $\delta^{15}N$-nitrate values exceeding 40‰ (Prouty et al., 2017a). Elevated $\delta^{15}N$ values were also recorded in corals adjacent to the seeps (Murray et al., 2019). The aragonite saturation values (Ω_{arag}) of the SGD are low or even under-saturated, with Ω_{arag} values ranging from 0.52–3.19 (Prouty et al., 2017a). In comparison, the water above the seeps is mixed with ambient seawater and registered a Ω_{sw} value of 2.9 during low tide. SGD at the seeps is also a source of elevated DIC (2600 μmol kg^{-1}) compared to ambient seawater (Prouty et al., 2018).

A second core was collected at Kahekili Beach Park from a coral head (LobataHead05) approximately 780 m north of the SSG in a water depth of less than 2 m (Fig. 1). While no active SGD seep clusters were detected at this site (Glenn et al., 2013), this site is within the northern extent of the warm SGD injectate plume as documented by infra-red thermal data and elevated algae $\delta^{15}N$ (12‰) and nitrate $\delta^{15}N$ (17‰) values (Dailer et al., 2010; Dailer et al., 2012; Hunt Jr. and Rosa, 2009). The pH range at this site was between 7.85 and 7.95 (Dailer et al., 2010; Hunt Jr. and Rosa, 2009), and dissolved inorganic nitrogen less than 5 μmol L^{-1} (Hunt Jr. and Rosa, 2009). While less in-situ data are available from this site, other sites that were sampled away from the SSG are dominated by strong mixing of seepage water with ambient seawater causing a mixing gradient with corals growing closer to the seep experiencing a stronger influence from SGD compared to the coral heads farther away. For example, at a sampling site 200 m from the SSG, SST ranged between 23.0 and 24.3 °C, salinity from 33.5 to 37.9, DIC from 1963 to 2083 μmol kg^{-1}, and Ω from 2.85 to 3.24 (Prouty et al., 2018).

At the control site in Olowalu Beach, south of Kahekili Beach Park, a coral core was collected from a water depth of 4.5 m (Prouty and Gallagher, 2017). Located approximately 13 km south of the main study in Kahekili Beach Park, this site is considered a control site given no major seepage was detected (Glenn et al., 2013). At this control site, temperature and salinity were recorded by a YSI sensor deployed at the coral head between October 17, 2012, and July 9, 2013. Monthly average temperatures fluctuated between 23.9 and 26.1 °C and salinity ranged between 33.0 and 34.4 (Storlazzi, USGS, written commun., 2021). Water quality parameters sampled from Olowalu Beach indicate a pH range from 7.92 to 8.03 (Glenn et al., 2013), with average nitrate concentration of 0.10 ± 0.5 μmol L^{-1} (Falinski et al., 2017).

2.2. Coral and calcifying fluid analysis

Using the density banding as a guide, carbonate boron analysis ($\delta^{11}B$ and B/Ca) was conducted along the major growth axis of coral cores (Supplemental Fig. S1). Measurements were carried out at GEOMAR, Helmholtz Centre of Ocean Research in Kiel, Germany, using an ESI New Wave Research UP193FX excimer laser, operating at 193 nm, connected to a Thermo Fisher (former VG) Axiom MC-ICP-MS, following the analytical procedures published in Fietzke et al. (2010) and Wall et al. (2019b). The ICP was operated at hot plasma (NAI 11–14) to provide stable matrix-independent measurement conditions (Fietzke and Frische, 2016). Sampling was conducted using a 150 μm spot size run as line scan at 300 μm s^{-1}. Scans were repeated five times along parallel tracks separated with 120 μm spacing, and the pattern was repeated in 18 runs. All 18 runs were integrated pixel-wise, scanning the same areas on the coral sample. Final $\delta^{11}B$ and B/Ca (estimated from B/C data) data represent the average of the five lines parallel tracks (e.g., first pixels of each line integrated, 2nd pixels of each line integrated, etc.). Results of four $\delta^{11}B$ standards (JCp-1, JCt-1, NIST610 and NBS951) measured repeatedly during the analytical sessions agree well with published values (Supplemental Table S1), yielding a $\delta^{11}B_{carb}$ precision of 1‰. Seawater analyses for $\delta^{11}B$ were performed on four samples collected at the SSG during both low and high tide, and two samples north of the SSG. The seawater samples were purified with anionic exchange resin and analyzed on a Thermo Finnigan Neptune MC-ICPMS following standard procedures (e.g., Foster, 2008; Stewart et al., 2021). The precision in $\delta^{11}B_{sw}$ was 0.2‰ (2SD) for 5 ng B. Accuracy was tested using

NIST RM 8391 (14.51 ± 0.15‰) and JCp-1 (24.22 ± 0.10‰). These values are within the range of recent inter-comparison efforts (Gutjahr et al., 2021; Stewart et al., 2021).

The equation of Zeebe and Wolf-Gladrow (2001) was used to calculate pH_{CF} based on measured coral $\delta^{11}B$ composition:

$$pH_{CF} = pK_B - log\left[-\left(\delta^{11}B_{sw} - \delta^{11}B_{carb}\right)/\left(\delta^{11}B_{sw} - \alpha_{(B3-B4)}\delta^{11}B_{carb}\right) - 1000\left(\alpha_{(B3-B4)} - 1\right)\right] \quad (1)$$

where $\delta^{11}B_{sw}$ is the $\delta^{11}B$ composition measured in two ambient seawater samples on the reef flat offshore of the SSG (40.01 ± 0.05‰) and $\delta^{11}B_{carb}$ is the $\delta^{11}B$ of boron inclusion of the carbonate, $\alpha_{(B3\text{-}B4)} = 1.0272$ (Klochko et al., 2006) is the boron isotope fractionation factor, and pK_B is the dissociation constant of boric acid in seawater dependent on the temperature and salinity (Dickson, 1990). The $\delta^{11}B$ composition in bottom water at the SSG during both low and high tide (39.94 ± 0.10‰) are similar to the ambient seawater. Given the lack of continuous in-situ SSS and SST time-series, average satellite derived SST (25.2 ± 0.3 °C) and SSS (34.3 ± 0.9) values were used over the length of the coral records, providing a minimum estimate in pH_{CF}. The reason for this is that the satellite data tend to underestimate site specific seawater temperature and overestimate seawater salinity at the SSG, resulting in lower pK_B values and thus pH_{CF} (by ~0.3 for both). Time series of CF pH, $[CO_3^{2-}]$ and DIC were calculated using combined carbonate $\delta^{11}B$ and B/Ca systematics with the computer code from DeCarlo et al. (2018). This script was run using 1000 Monte Carlo simulations to estimate the non-systematic error for the CF pH, $[CO_3^{2-}]$ and DIC outputs (Tables 1a, 1b and 2; Supplemental Figs. S2, S3). The choice of partition coefficient (K_D) between aragonite and seawater influences the application of boron systematics given the dependency of K_D on fluid chemistry (Allison, 2017; Holcomb et al., 2016; Trotter et al., 2011). Three different K_D formulas were considered (Supplemental Fig. S4). We used the K_D formula from McCulloch et al. (2017) because the resulting $[CO_3^{2-}]_{CF}$ and DIC_{CF} values were generally less than those from the other two options (Holcomb et al., 2016; and DeCarlo et al., 2018) and was therefore chosen as a more conservative approach. A one-way analysis of variance (ANOVA) test indicates that there was no statistical difference between the outputs from the different K_D options, except in the case of $[CO_3^{2-}]_{CF}$ from LobataHead06. For this single case the DeCarlo et al. (2018) K_D approach resulted in $[CO_3^{2-}]_{CF}$ values whose mean and distributions were statistically different from the McCulloch et al. (2017) method. However, even in this case, the RMSE between these two $[CO_3^{2-}]_{CF}$ outputs was less than the maximum error associated with the $[CO_3^{2-}]_{CF}$ calculation (51.9 compared to 199.5 μmol kg^{-1}); thus, it seems reasonable to conclude that the choice of K_D method is not important to the computed $[CO_3^{2-}]_{CF}$ and DIC_{CF} values relative to the overall uncertainty, similar to recent results from a cross-Pacific study (Thompson et al., 2022).

The aragonite saturation state (Ω_{arag}) of the CF was calculated using an Excel Workbook Macro translation of the original CO2SYS program (Pierrot et al., 2006) and is defined as the product of $[CO_3^{2-}]$ and $[Ca^{2+}]$ divided by the aragonite solubility product (K_{sp}). Without in-situ calcium data, the concentration was assumed to be proportional to changes in salinity (34.3) and applied with a $[Ca^{2+}]$ of 10 mmol L^{-1} and the carbonate concentration was calculated from pH and DIC (derived from $\delta^{11}B$ and B/Ca respectively), and the values of K_1 and K_2 (Pierrot et al., 2006). The CO2SYS 2.0 program was run with dissociation constants K_1 and K_2 from Mehrbach et al. (1973) refit by Dickson and Millero (1987) and K_{SO4} from Dickson (1990), and boron-derived proxies for pH_{CF} and DIC_{CF}, average nutrient data at the SSG (0.21 μmol L^{-1} PO_4^{3-} and 10.45 μmol L^{-1} Si) and away from the seep site (0.09 μmol L^{-1} PO_4^{3-} and 2.81 μmol L^{-1} Si) (Prouty et al., 2017b; Prouty et al., 2018), and satellite-derived-SST and salinity. The time-varying uncertainties associated with the Ω_{arag} values were determined using the Pierrot et al. (2006) MATLAB CO2SYS 2.0 package (https://www.ncei.noaa.gov/access/ocean-carbon-acidification-data-system/oceans/CO2SYS/co2rprt.html). These errors are shown in Supplemental Figs. S2, S3, S5, and the maximum errors are given in Tables 1a, 1b, and 2.

According to the bio-inorganic model (IpHRAC) of McCulloch et al. (2012a), gross calcification rates were calculated from boron derived calcifying fluid conditions using the empirical exponential rate dependence law for carbonate precipitation from Burton and Walter (1987):

$$G = K(\Omega_{CF} - 1)^n \quad (2)$$

with the temperature-dependence for aragonite precipitation:

$$K = -0.0177\,T^2 + 1.47\,T + 14.9 \quad (3)$$

$$n = 0.0628\,T + 0.0985 \quad (4)$$

and Ω_{CF} derived from skeletal derived boron signature and temperature in Kelvin.

2.3. NMR analysis

High field ^{11}B magic angle spinning nuclear magnetic resonance (^{11}B MAS NMR) spectroscopy was used to investigate the different species of boron, specifically borate tetrahedral form (BO_4) and boric acid trigonal (BO_3) (Klochko et al., 2006; Rollion-Bard et al., 2011), in selected coral samples from Kahekili Beach Park. Discretely drilled coral samples (~60 mg) were selected at eight time periods over the lifespan of each coral for NMR analysis. The ^{11}B MAS/NMR spectra were acquired at 160.3 MHz with a 500 MHz (11.7 T) Varian Infinityplus spectrometer and Chemagnetics-type probe assembly configured for 3.2 mm (o.d.) rotors. A spinning rate of 8 kHz was employed for all ^{11}B NMR experiments. Excitation was provided by 1 μs pulses of a 50 kHz transverse field, corresponding to a 5 μs non-selective 90° pulse. Each spectrum represents $0.5{\cdot}10^6$–$1.6{\cdot}10^6$ scans, separated by a 0.15 s relaxation delay.

Table 1a
Range (minimum, maximum, average, and standard deviation) of boron systematics ($\delta^{11}B$ and B/Ca) from north of the South Seep Group (LobataHead05), calculated calcifying fluid carbonate parameters (pH_{CF}, DIC_{CF}, $[CO_3^{2-}]_{CF}$ and Ω_{CF}), maximum errors, seasonal range (average and standard deviation), and difference (average and standard deviation) between carbonate and seawater composition (ΔSW) and magnitude of up-regulation expressed as "x" times seawater. Gross calcification rates calculated according to the bio-inorganic model (IpHRAC) of McCulloch et al. (2012a). *Average seawater composition from Prouty et al. (2017a, 2018).

LobataHead05	$\delta\ ^{11}B_{carb}$ ‰	B/Ca_{carb} μmmol mol^{-1}	pH_{CF}	$[CO_3^{2-}]_{CF}$ μmol kg^{-1}	DIC_{CF} μmol kg^{-1}	Ω_{CF}	Gross calcification rate mg cm^{-2} yr^{-1}
Min.	24.0	291	8.5	1276	3626	20.2	5.1
Max.	31.3	501	8.9	2178	7161	34.4	13.0
average	28.5	422	8.8	1711	4512	27.0	8.6
±SD	1.2	36	0.1	144	522	2.3	1.3
Max. error	0.2	10	7×10^{-2}	182	312	4.1	
Seasonal range	3.1	64.4	0.2	430	1056	7.3	–
±SD	0.8	24.7	0.1	166	355	3.5	–
Seawater*	–	–	8.0	193	1999	3	–
ΔSW	n.a.	n.a.	0.8	1513	2499	23.9	–
±SD	n.a.	n.a.	0.1	187	538	2.5	–
x SW	n.a.	n.a.	1×	9×	2×	9×	–

Table 1b
Range (minimum, maximum, average, and standard deviation) of boron systematics ($\delta^{11}B$ and B/Ca) at the South Seep Group (LobataHead06), calculated calcifying fluid carbonate parameters (pH_{CF}, DIC_{CF}, $[CO_3^{2-}]_{CF}$ and Ω_{CF}), maximum errors, seasonal range (average and standard deviation), and difference (average and standard deviation) between carbonate and seawater composition (ΔSW) and magnitude of up-regulation expressed as "x" times seawater. Gross calcification rates calculated according to the bio-inorganic model (IpHRAC) of McCulloch et al. (2012a). *Average seawater composition from Prouty et al. (2017a, 2018).

LobataHead06	$\delta^{11}B_{carb}$ ‰	B/Ca_{carb} μmol mol^{-1}	pH_{CF}	$[CO_3^{2-}]_{CF}$ μmol kg^{-1}	DIC_{cF} μmol kg^{-1}	Ω_{CF}	Gross calcification rate mg cm^{-2} yr^{-1}
Min.	26.4	297	8.6	1478	3810	23.2	6.6
Max.	31.6	460	9.0	2782	6431	43.7	19.6
Average	29.3	392	8.8	1932	4752	30.5	10.6
±SD	1.1	31	0.1	169	473	2.7	1.6
Max. error	0.2	10	8×10^{-2}	200	310	5.0	
Seasonal Δ	2.9	70.8	0.2	391	942	5.9	–
±SD	0.9	23.1	0.1	135	434	2.3	–
Seawater	–	–	8.0	193	1999	3	–
ΔSW	n.a.	n.a.	0.8	1734	2684	27.2	–
±SD	n.a.	n.a.	0.1	221	504	3.1	–
x SW	n.a.	n.a.	1×	10×	2×	10×	–

Table 2
Average (±SD) values and maximum errors of the boron systematics ($\delta^{11}B$ and B/Ca) at the control site (Olowalu Beach), and calculated calcifying fluid carbonate parameters (pH_{CF}, DIC_{CF}, $[CO_3^{2-}]_{CF}$ and Ω_{CF}), and gross calcification rate.

Olowalu beach variable	Average (±SD)	Max. error
$\delta^{11}B_{carb}$	23.7 ± 1.8‰	
B/Ca_{carb}	349 ± 20 μmol mol^{-1}	
$[CO_3^{2-}]_{CF}$	1387 ± 234 μmol kg^{-1}	179
DIC_{cF}	5980 ± 396 μmol kg^{-1}	280
pH_{CF}	8.4 ± 0.1	0.1
Ω_{CF}	21.8 ± 3.7	3.9
Gross calcification	6.0 ± 1.8 mg cm^{-2} yr^{-1}	

Additional spectra of some samples taken with a 1 s relaxation delay showed no substantial differences and indicate that 75–80% of the equilibrium magnetization is returned with the shorter relaxation time. Differential relaxation effects could impart minor deviations of the integrated peak intensities from population ratios, up to about 2%. The ^{11}B MAS/NMR experiments for empty rotor assemblies yielded signal below the detection limit ($S/N < 3$). Chemical shifts are reported with respect to neat boron trifluoroetherate via an external datolite standard, the peak position of which was set to 0.17 ppm at 11.7 T (Hansen et al., 2004). Chemometrics analysis of the NMR data was performed to decompose and extract relevant spectral information and calculate percent contribution from boron species (Mason et al., 2012).

3. Results

3.1. Boron systematics and carbon isotopes

Monthly coral $\delta^{11}B$ and B/Ca variability was clearly observed in both coral records from Kahekili Beach Park, (Fig. 2). Coral $\delta^{11}B$ at the SSG (LobataHead06) range from 26.4 to 31.6‰ with an average (±SD) value of 29.3 ± 1.1‰ and for the coral collected to the north of the SSG from 24.0 to 31.3‰ with an average (±SD) value of 28.5 ± 1.2‰. Coral B/Ca values at the SSG ranged from 297 to 460 μmmol mol^{-1} with an average (±SD) value of 392 ± 31 μmmol mol^{-1} and from 291 to 501 μmmol mol^{-1} with an average (±SD) value of 422 ± 36 μmmol mol^{-1} at the northern site (Table 1). Coral boron systematics at the control site are distinct from the results reported above for the impacted study region of Kahekili Beach Park. At Olowalu Beach, coral $\delta^{11}B$ ranged from 17.9 to 28.8‰ with an average (±SD) value of 23.7 ± 1.8‰ (Table 2, Supplemental Fig. S5). Coral B/Ca values ranged from 310 to 487 μmmol mol^{-1} with an average (±SD) of 349 ± 20 μmmol mol^{-1}.

The Kahekili Beach Park coral boron data time-series are dominated by variability in the interannual to sub annual timescale (Fig. 2, Supplemental Figs. S6 and S7). At the SSG (LobataHead06), the first principal component accounts for 65 and 67% of the total variance in the $\delta^{11}B$ and B/Ca time-series, respectively (Table 3). At the northern site (LobataHead05), 82% of the B/Ca variance is explained by an annual signal, whilst the $\delta^{11}B$ time-series is characterized by a dominant period of 1.8 years and accounts for 66% of the variance (Table 3).

Coral $\delta^{13}C$ values at Kahekili Beach Park ranged from −3.28 to 0.38‰ with an average (±SD) isotopic composition of −1.59 ± 0.65‰ at the north site, whereas at the SSG site the coral samples were ^{13}C-enriched, exhibiting a range from −1.95 to 1.55‰ with an average (±SD) $\delta^{13}C$ value of −0.23 ± 0.59‰ (Supplemental methods; Supplemental Fig. S8). For comparison, coral tissue and particulate organic carbon $\delta^{13}C$ values from the reef flat were lower and varied from −5.12 to −2.77‰ and − 26.9 to −21.32‰, respectively. Coral $\delta^{18}O$ values were similar at the two Kahekili Beach Park sites ranging from −4.73 to −3.07‰ at the SSG site to −4.53 to −3.73‰ at the northern site. Spectral analysis of the isotope data captures an annual component in the coral stable isotope time-series at the northern site (Supplemental Fig. S6), whereas $\delta^{13}C$ and $\delta^{18}O$ at the SSG site yield a longer periodic component (2.2 yrs.) (Supplemental Figure S7), which could potentially be an artifact of a minor age error. Coral $\delta^{13}C$ and $\delta^{18}O$ components are in phase with each other yet do not exhibit a clear phase relationship with pH_{CF}.

3.2. Calcifying fluids

Results from Single Spectrum Analysis (SSA) of the boron-derived carbonate chemistry time-series (see Supplemental Methods) mimic the $\delta^{11}B$ and B/Ca data and display similar frequency behavior to the PSD (Supplemental Figs. S6 and S7). At both Kahekili Beach Park sites DIC_{CF} exhibits annual periodicity as does pH_{CF} at the SSG site whereas pH_{CF} at the northern site has a dominant periodic component of 1.8 yrs., mirroring the $\delta^{11}B$ record (Table 3). Variability in the chemistry of the CF, including pH_{CF}, DIC_{CF}, $[CO_3^{2-}]_{CF}$ and Ω_{CF} was calculated as described above and the range and average (±SD) values are reported in Table 1. Average (±SD) pH_{CF} value at both sites was 8.8 ± 0.1, average (±SD) DIC_{CF} values were 4752 ± 473 μmol kg^{-1} at the SSG and 4512 ± 522 μmol kg^{-1} at the northern site, and Ω_{CF} values were 30.5 ± 2.7 at the SSG and 27.0 ± 2.3 at the northern site. In contrast to the Kahekili Beach Park cores, average (±SD) pH_{CF} from the control site at Olowalu Beach was 8.4 ± 0.1, 0.40 pH units lower. The average (±SD) DIC_{CF} value was 5980 ± 396 μmmol kg^{-1}, higher compared to Kahekili Beach Park, while calculated Ω_{CF} values were lower at Olowalu Beach with an average (±SD) value of 21.8 ± 3.7.

The average (±SD) seasonal range (i.e., difference between the minimum and maximum values over a given year) at Kahekili Beach Park for pH_{CF} was between 0.20 ± 0.06 and 0.22 ± 0.05 (Table 3), which is similar to the diurnal seawater pH range at the study site (Prouty et al., 2018) and the seasonal pH range along the reef flat (Glenn et al., 2013). The average (±SD) seasonal range in Ω_{CF} is 5.94 ± 2.26 and 7.26 ± 3.54 at the SSG and north site, respectively, which is an

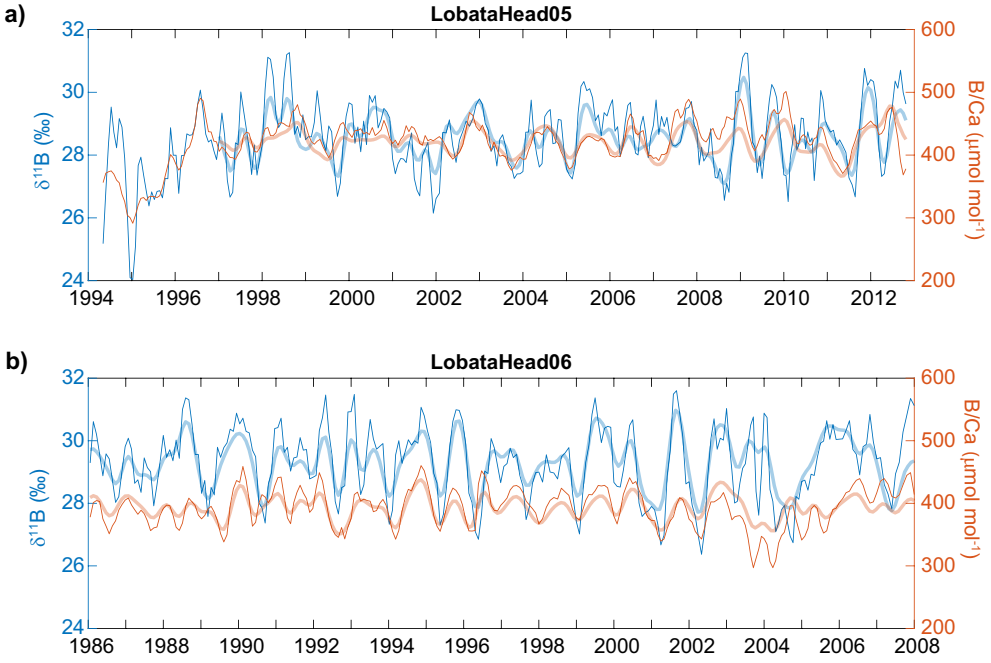

Fig. 2. Time-series of coral boron isotope ($\delta^{11}B$; blue) and boron:calcium ratios (B/Ca; orange) from a) LobataHead05 north of the South Seep Group and b) LobataHead06 at the South Seep Group. The first principal component reported in Table 2 is plotted as thicker line. (For interpretation of the references to colour in this figure legend, the reader is referred to the web version of this article.)

Table 3
Dominant periods and percent variance explained by the first principal component identified in Singular Spectrum Analysis (SSA), described further in the Supplemental Methods.

Variable	LobataHead05	LobataHead06
$\delta^{11}B_{carb}$	1.8 yr (66%)	1.3 yr (65%)
B/Ca_{carb}	1.3 yr (82%)	1.5 yr (67%)
$[CO_3^{2-}]_{CF}$	1.5 yr (69%)	1.8 yr (63%)
DIC_{CF}	1.3 yr (81%)	1.3 yr (68%)
pH_{CF}	1.8 yr (71%)	1.3 yr (65%)
Ω_{CF}	1.5 yr (68%)	1.8 yr (62%)
$\delta^{13}C_{carb}$	1.2 yr (83%)	2.2 yr (76%)
$\delta^{18}O_{carb}$	1.3 yr (69%)	2.2 yr (71%)

order of magnitude larger than the diurnal seawater range in Ω_{sw}. Seasonal Ω_{sw} data are not available from this region nor from Olowalu Beach. The seasonal range in CF carbonate chemistry parameters is similar between the Kahekili Beach Park sites (Student *t*-test; $p > 0.05$), with the exception of DIC_{CF} where the range at the SSG is 942 ± 434 μmmol kg^{-1} versus 1056 ± 355 μmol kg^{-1} at the northern site, and it is much larger than the diurnal seawater range on the reef flat (<200 μmol kg^{-1}) (Prouty et al., 2018). The larger range calculated at the north site may be disproportionally influenced by one anomalous high DIC_{CF} measurement (7000 μmol kg^{-1}) during the early record (1985), derived from a lower coral $\delta^{11}B$ and B/Ca (Fig. 2). Omitting this value reduces the average seasonal range at this site to 848 ± 225 μmol kg^{-1}. There is an inverse relationship between DIC_{CF} and pH_{CF} at the Kahekili Beach Park sites ($r = -0.56$; $p < 0.01$ SSG; $r = -0.65$; $p < 0.01$ north) (Table 3) (Tables 4a and 4b), as shown in Fig. 3. Cross spectral analysis of the first component of the SSA confirms the DIC_{CF} and pH_{CF} antiphase relationship are out-of-phase (180°).

The DIC_{CF} and $[CO_3^{2-}]_{CF}$ concentrations at Kahekili Beach Park are ~2× seawater and 9–10× seawater values, respectively (Table 1). Calculated Ω_{CF} values range from 23.2 to 43.7 at the SSG and 20.2 to 34.4 to the north. These values indicate Ω_{CF} conditions that are on average 9 to 10× higher than the ambient seawater Ω values. At both Kahekili Beach Park sites the CF carbonate chemistry parameters are higher relative to seawater, however at the SSG site the absolute pH values are only slightly higher and the offsets (e.g., ΔpH) are larger.

Using the Ω_{CF} derived from skeletal derived boron data, the average gross calcification rates were calculated as 12,100 at the SSG and 9800 μmol m^{-2} h^{-1} at the north site, equivalent to 10.6 and 8.6 mg cm^{-2} yr^{-1}, respectively (Table 1), whereas average gross calcification at the control site a Olowalu Beach is almost twice as low relative to the SSG, 6800 μmol m^{-2} h^{-1} (6.0 mg cm^{-2} yr^{-1}).

3.3. Boron speciation

The ^{11}B NMR spectra are dominated by a single peak centered near 0.8 ppm with a width of 2.4–2.8 ppm FWHM (Fig. 4). This peak position and relatively narrow width are consistent with assignment to 4-coordinated $B(O)_4$ groups (Turner et al., 1986), and are similar to previous

Table 4a
Pearson-product correlation coefficients (r; $p < 0.01$) between coral boron systematics ($\delta^{11}B$ and B/Ca) from north of South Seep Group (LobataHead05), calculated calcifying fluid carbonate parameters (pH_{CF}, DIC_{CF}, $[CO_3^{2-}]_{CF}$ and Ω_{CF}), and calculated gross calcification.

LobataHead05	B/Ca_{carb}	$[CO_3^{2-}]_{CF}$	DIC_{cF}	pH_{CF}	Ω_{CF}	Gross Calcification
$\delta^{11}B_{carb}$	0.48	0.37	−0.66	–	0.36	0.19
B/Ca_{carb}		−0.40	−0.88	0.48	−0.48	−0.20
$[CO_3^{2-}]_{CF}$			0.20	0.37	0.65	0.34
DIC_{cF}				−0.65	0.42	0.18
pH_{CF}					0.36	0.19
Ω_{CF}						0.69

Table 4b
Pearson-Product Correlation Coefficients (r; $p < 0.01$) between coral boron systematics ($\delta^{11}B$ and B/Ca) at the South Seep Group (LobataHead06), calculated calcifying fluid carbonate parameters (pH_{CF}, DIC_{CF}, $[CO_3^{2-}]_{CF}$ and Ω_{CF}), and calculated gross calcification.

LobataHead06	B/Ca_{carb}	$[CO_3^{2-}]_{CF}$	DIC_{cF}	pH_{CF}	Ω_{CF}	Gross Calcification
$\delta^{11}B_{carb}$	0.40	0.39	−0.56	–	0.42	0.26
B/Ca_{carb}		−0.45	−0.87	0.40	−0.52	−0.34
$[CO_3^{2-}]_{CF}$			0.27	0.39	0.67	0.41
DIC_{cF}				−0.56	0.47	0.26
pH_{CF}					0.42	0.26
Ω_{CF}						0.77

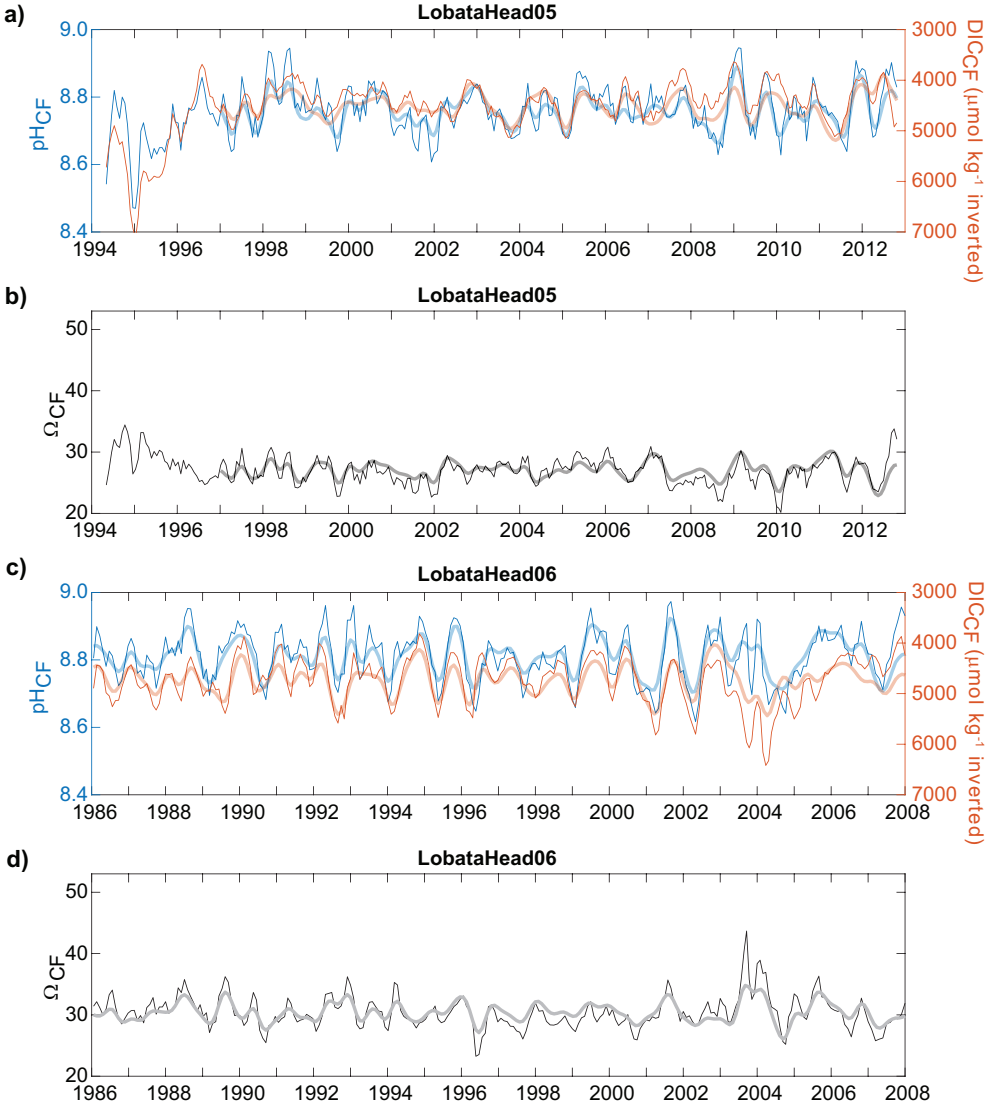

Fig. 3. Time-series of a) pH_{CF} (blue), DIC_{CF} (orange; y-axis inverted) and b) Ω_{CF} (black) from LobataHead05 north of the South Seep Group and c) pH_{CF} (blue), DIC_{CF} (orange; axis inverted) and d) Ω_{CF} (black) from LobataHead05 at the South Seep Group. The first principal component reported in Table 2 is plotted as thicker line. (For interpretation of the references to colour in this figure legend, the reader is referred to the web version of this article.)

reports for ^{11}B MAS/NMR spectra of synthetic and coral aragonite (Mavromatis et al., 2015; Rollion-Bard et al., 2011; Sen et al., 1994). In addition to the narrow peak at 0.8 ppm, the spectrum of raw material from the upper portion (7 mm) of skeletal growth from LobataHead05 also contains peaks at 9.1 and 4.6 ppm that are absent from a spectrum taken after treatment with a NaOCl solution (Supplemental Fig. S9). Smaller peaks at similar positions are apparent in spectra of several other samples. The relatively narrow widths of these additional peaks indicate the quadrupolar coupling constants are small, consistent with 4-coordinated boron.

4. Discussion

4.1. Up-regulation

A key finding of this study is that coral $\delta^{11}B_{carb}$ values at Kahekili Beach Park are higher (28.5 to 29.3‰) relative to those at the control site at Olowalu Beach (23.7 ± 1.78‰) and tend to increase toward the

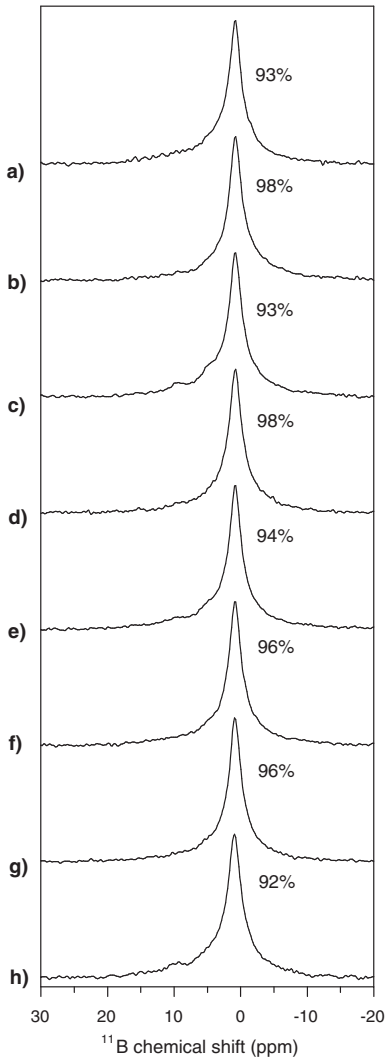

Fig. 4. Centerband region of ^{11}B MAS/NMR spectra of powdered *Porites* spp. from Kahekili Beach Park of LobataHead05 north of the South Seep Group from a) 1994 b) 2000 c) 2006 and d) 2012; and LobataHead06 at the South Seep Group from e) 1969 f) 1989 g) 1998 and CF) 2007. Data acquired at 11.7 T and 8 kHz spinning rate, using 1 μs pulses and 0.15 s relaxation delay for 500,000-1,600,000 acquisitions. Spinning sidebands lie outside the displayed spectral region. The large peak at 0.8 ppm indicates the dominance of tetrahedral boron (BO_4) with percent contribution from borate shown for each sample.

main effluent regions. Additionally, those values exceed reported values in the literature and from other locations in Hawai'i for *Porites* spp. Based on previous work, typical shallow coral $\delta^{11}B_{carb}$ values range between 20.41 and 26.03‰ (Allison et al., 2014; Allison and Finch, 2010; D'Olivo and McCulloch, 2017; Douville et al., 2010; McCulloch et al., 2018; McCulloch et al., 2017; Wall et al., 2019a; Thompson et al., 2022). For example, the average $\delta^{11}B_{carb}$ values in *P. lobata* from Lanikai, Oahu, 25.2 ± 1.8‰, 24.14 ± 0.20‰ in *P. compressa* from Kane'ohe Bay in Oahu, Hawai'i (Andersson et al., 2020), and less than 25.5‰ in *P. compressa* from Kane'ohe Bay and Waimanalo Bay, Hawai'i (Schoepf et al., 2017). These data agree with our control site. The anomalously high $\delta^{11}B_{carb}$ values from Kahekili Beach Park suggest some systematic differences in the physiological CF regulation or mechanisms of B incorporation into the CF in the SSG corals derived from the wastewater impact. Site specific $\delta^{11}B$ values of the water in which the coral grows can influence pH_{CF} as these waters are the source of the boron in the calcifying fluid (Eq. (1)). However, the $\delta^{11}B$ composition in bottom water at the SSG during both low and high tide (40.01 ± 0.05‰) and in ambient seawater north of the SSG (39.94 ± 0.10‰) are only slightly higher than values in the open ocean 39.61 ± 0.04‰ (Foster et al., 2010) and hence source water $\delta^{11}B$ variability cannot explain elevated $\delta^{11}B_{carb}$ at Kahekili Beach Park. Changes in DIC_{sw} can also influence CF composition. For example, Gagnon et al. (2021) found a systematic decrease in $\delta^{11}B$ of −1.08‰ per mmol kg^{-1} change in DIC_{sw} in cold-water corals. They argued that this $\delta^{11}B$ decrease is a function of increased boric acid diffusion across coral cell membrane that thereby provide a ^{11}B-enriched source to the CF. While boric acid diffusion could distort the $\delta^{11}B$ signal and mask the ability to derive CF carbonate chemistry, this scenario contrasts with observations of directly measured higher pH_{CF} value in cultured *Stylophora pistillata* exposed to elevated DIC_{sw} (Comeau et al., 2017). Furthermore, since SGD at our site is a source of additional DIC, the model proposed by Gagnon et al. (2021) would dictate a $\delta^{11}B$ decrease, opposite of what is observed in the Kahekili Beach Park $\delta^{11}B$ coral values and could only be compensated by even higher pH upregulation.

4.2. Incorporation of borate ion

Other ways in which coral $\delta^{11}B$ values could be altered include the incorporation of boric acid into the aragonite precipitate (Farmer et al., 2019). Incorporation of boric acid into aragonite crystal, however, appears negligible (<15%; Mavromatis et al., 2015; Noireaux et al., 2015), and previous studies indicate that the presence of boric acid does not seem to be associated with an isotope effect (Noireaux et al., 2015). Results from the NMR analysis confirm that boron is predominantly present as borate with no evidence of boric acid (Hemming and Hanson, 1992). The increased chemical shifts of the minor peaks near +9.1 and +4.6 ppm relative to those typical for borate ion and tetrahedral boron in oxide materials suggest assignment to organoboron complexes (e.g., Bishop et al., 2004), which is consistent with the absence of these peaks in spectra taken after treatment with an oxidizing solution. This observation indicates some tissue material might have been taken up during microdrill sampling of the skeletal material given this period of growth coincides with the organic rich tissue layer.

Although some previous studies have reported significant fractions of boron in coral aragonite occurring as 3-coordinated $B(O)_3$ species (Klochko et al., 2009; Rollion-Bard et al., 2011), the present results show no evidence for such species in the samples examined here. Under the NMR experimental conditions of this study, trigonal boron would yield signal in the range from 16 to 8 ppm, based on the isotropic chemical shifts (17–18 ppm) and quadrupolar coupling constants (2.3–2.5 MHz) previously reported. Second-order quadrupolar effects significantly broaden the MAS/NMR peak shape for trigonal boron, shifting intensity from the isotropic chemical shift toward lower chemical shifts. Spectral features observed near 10 ppm for the samples investigated here can be accounted for by smaller proportions of the peaks from the organoboron species most evident in the spectrum of the upper portion of LobataHead06 taken prior to cleaning. Furthermore, intensity in the 16–8 ppm chemical shift range cannot be simulated by calculated MAS/NMR peak shapes using the NMR parameters determined previously for trigonal B in coral aragonite (Klochko et al., 2009; Rollion-Bard et al., 2011) or those calculated for proposed defect structures (Balan et al., 2016). Absence of signal from trigonal boron is further supported by a model-free chemometric decomposition of the spectral series in Fig. 4, using the methods described by Mason et al. (2012). The results show that the spectra can be reproduced with just two components in varying proportions, one consisting of a narrow peak at +0.8 ppm and a second containing symmetrical peaks at 9.1, 4.6, and 0.8 ppm (Supplemental Fig. S10). The residuals consist only of random noise in the chemical shift range 16 to 8 ppm, with no coherent signal that could be attributed to trigonal B. Therefore, neither diffusion or incorporation of boric acid is sufficient to explain the elevated Kahekili Beach Park $\delta^{11}B_{carb}$ values and therefore other biological and environmental drivers must be the drivers of the pH up-regulation.

4.3. Abiotic factors and coral physiology

Abiotic factors such as salinity and temperature can also influence pH_{CF} values given the sensitivity of pK_B to changes in salinity and temperature. However, adjusting pK_B in the calculations for site specific temperature and salinity in this case would result in an even higher pH_{CF} as explained earlier. Another way by which $\delta^{11}B_{CF}$ can be altered is through changes in $[Ca^{2+}]_{sw}$. Experiments by Giri et al. (2019) demonstrate that under high $[Ca^{2+}]_{sw}$ conditions, the amount of Ca^{2+} actively taken into the CF (Ca^{2+}-pumping) is lower, resulting in higher B/Ca ratios but lower pH_{CF} values. Therefore, the reverse is plausible if SGD limits the available calcium ions needed for the Ca-ATPase pump. However, given the high concentration of calcium in seawater, SGD will have a minimal impact on the available calcium ions, suggesting a negligible impact on the Ca-ATPase pump and $\delta^{11}B_{CF}$.

Coral physiology must also be considered when exploring mechanisms to explain CF pH up-regulation. Previous work has suggested that pH_{CF} increases to compensate for lower photosynthesis-driven supply of metabolic DIC_{CF} (D'Olivo and McCulloch, 2017; McCulloch et al., 2017). At a seasonal scale this explanation appears valid. At Kahekili Beach Park pH_{CF} and DIC_{CF} are negatively correlated, which may reflect increased pH_{CF} in the winter to compensate for reduced photosynthesis-driven supply of metabolic DIC_{CF}, while less pH up-regulation is required in the summer when photosynthesis is heightened. This anti-phase relationship between pH_{CF} and DIC_{CF} was also observed in corals from the Great Barrier Reef where temperature- or light-driven changes in the supply of metabolic DIC provided by the endosymbionts was linked to seasonal to-annual trends in pH_{CF} and DIC_{CF} (D'Olivo and McCulloch, 2017; McCulloch et al., 2017).

While seasonality follows common patterns it does not explain the overall shift toward higher $\delta^{11}B_{carb}$ values, which may be linked to chronic compound stressors (e.g., nutrient and sediment loading) that further may modulate physiological performance. Chronic stressors may distort the balance between host and symbiont and potentially disrupt the supply of DIC by the endosymbionts. While changes in thermal conditions is considered a trigger for negatively impacting symbiotic algae, corals actively regulate their symbiont density in response to other environmental conditions that can cause physiological stress, including nutrient imbalance (Morris et al., 2019; Pogoreutz et al., 2017; Rosset et al., 2017; Vega Thurber et al., 2014). For example, disruption of the symbiotic partnership is largely attributed to increased nitrogen, whereby increase nitrate assimilation encourages symbiont parasitism (Baker et al., 2018). In turn, disruption of the symbiotic partnership can alter the supply of metabolic DIC, thereby triggering a change in pH up-regulation as part of the Ca-ATPase pump. Likewise, a greater reliance on heterotrophic feeding relative to autotrophy (i.e., photosynthesis) in eutrophic conditions could alter the supply of metabolic DIC. This interpretation assumes the symbionts activity result in the modulation of CF composition whereas removal of protons from the calcification site via Ca^{2+}-ATPase is controlled by coral enzyme production (e.g., Comeau et al., 2017). Therefore, excess nutrient loading may potentially affect enhanced pH up-regulation by altering the symbiotic alga photosynthetic DIC supply, and/or increase the contribution of heterotrophic feeding in response to nutrient availability as discussed below.

4.4. Compound stressors

Several factors, such as changes in seawater composition (pH, Ca, DIC) as well as changes in coral physiology, can influence $\delta^{11}B_{carb}$ and pH_{CF}. Other pollutants as pharmaceuticals, which have been detected on the reef (Campbell et al., 2017), may also impact coral physiology (Nalley et al., 2021). While it may be difficult to tease apart the specific mechanism without conducting laboratory experiments, previous work at Kahekili Beach Park has shown both primary and secondary effects of nutrient rich, lower pH effluent-SGD. These impacts include increased bioerosion rates and changes in carbonate chemistry along the reef flat, corroborating a previously suggested link between local wastewater injection and degradation of the reef environment that cannot be explained by changes in temperature or salinity. For example, during periods of increased SGD, Prouty et al. (2018) observed a shift in carbonate dynamics that favored respiration and dissolution relative to calcification and photosynthesis as captured in the increased DIC and total alkalinity (TA) values on the reef flat. This shift to negative net community calcification (-NCC) and negative net community productivity (-NCP) is attributed to a nutrient-driven increase in phytoplankton biomass and ensuing decomposing organic matter (Prouty et al., 2018). The dominance of net respiration (R) relative to photosynthesis (P) suggests that the coral-algal association consumed more energy than it produced during increase nutrient loading. The decrease in P:R ratio, as a proxy for autotrophic capacity, is also consistent with an increase in coral heterotrophic feeding relative to autotrophic feeding (Coles and Jokiel, 1977; Hughes and Grottoli, 2013) and observations that coral tissue thickness (i.e., stored lipid reserve) was negatively correlated to coral tissue $\delta^{15}N$ values ($r = -0.66$; $p = 0.08$), with the latter serving as a proxy for nutrient loading (Dailer et al., 2010). Thus, Prouty et al. (2018) suggested that a reduction in coral tissue reflects preferential heterotrophic feeding under high nutrient loading, with nutrient enrichment by sewage effluent increasing primary production and biomass in the water column (e.g., Pastorok and Bilyard, 1985; Smith et al., 1981). While the Kahekili Beach Park coral $\delta^{13}C$ data, as a tracer for carbon acquisition (McConnaughey, 1989; McConnaughey et al., 1997; Porter et al., 1989; Swart, 1983), are inconclusive, it is possible that excess nutrient loading is shifting reef metabolism and triggering up-regulation. In response, the corals are creating CF supersaturated with respect to aragonite conditions that are 9 to 10× greater than seawater (Ω_{CF} = 20–30), thereby employing a biological strategy to promote mineral precipitation in response to nutrient-driven calcification stressors. This response occurs year-round (superimposed on seasonal variability) since even the seasonally low $\delta^{11}B$ and pH_{CF} values are high relative to other *Porites* spp. values. Such elevated saturation conditions suggest higher gross calcification rates at SSG. This, however, is in contrast to the lower net calcification as well as linear extension rate reported from the CT analysis; net calcification and linear extension rate at the SSG were 0.68 g cm^{-2} yr^{-1} and 0.69 cm yr^{-1} compared to 1.02 cm^{-2} yr^{-1} and 0.95 cm yr^{-1} north of the SSG (Prouty et al., 2017a) and warrants further investigation. Measured coral bioerosion rates at Kahekili Beach Park, however, were up to 8 times greater than expected, suggesting that eutrophication of reef seawater can magnify the effects of OA through nutrient driven-bioerosion (Prouty et al., 2017a). Therefore, positive gains in gross calcification due to higher Ω_{CF} may be offset by both biological and chemical bioerosion as well as an imbalance between net carbonate accretion and net carbonate dissolution from exposure to nutrient-enriched, low pH SGD but not reflected in the corals extension rate.

5. Conclusions

A dual geochemical approach using $\delta^{11}B$ and B/Ca data suggests the corals exposed to low pH, high nutrient waters that have an effluent signature modify calcification rates over their ~20-year lifespan by creating calcifying fluid supersaturated with respect to aragonite conditions that are 9 -10× greater than seawater (Ω_{CF} = 20–30) and 13 to 26% higher than in corals from the control site, and from other *Porites* spp. studies. While several factors can influence coral boron systematics, including seawater composition and coral physiology, up-regulation provides a potential coping mechanism to respond to nutrient-driven calcification stressors, such as a shift in carbonate dynamics that favor respiration-dissolution processes relative to calcification-photosynthesis. Gross calcification rates are elevated relative to the control site; however, positive gains in gross calcification reported here are offset by both chemical and mechanical bioerosion. This offset may continue to expand given the vulnerability of reefs occupying densely

inhabited shorelines to coastal acidification and eutrophication, adding an additional stressor to thresholds tipping the balance between net carbonate accretion and net carbonate dissolution. Results from this study not only provide temporal and spatial information about the footprint of the nutrient-enriched, low pH injectate plume, but also provide insight into potential coral response to calcification stressors. Coral boron systematics offer an important tool in evaluating coral sensitivity to changes in coral reef conservation and management practices that influence water quality, especially as local conditions exacerbate global threats from rising SSTs and OA.

Supplementary data to this article can be found online at https://doi.org/10.1016/j.marchem.2022.104134.

Declaration of Competing Interest

None.

Acknowledgments

This research was carried out as part of the US Geological Survey's Coral Reefs Project in an effort in the United States and its trust territories to better understand the effects of geologic and oceanographic processes on coral reef systems and were supported by the USGS Coastal and Marine Hazards and Resources Program. We thank P. Swarzenski (USGS) and two anonymous reviewers for providing helpful comments that greatly improved the manuscript. Additional geochemical data to support this project can be found in Prouty and Fietzke (2021). Any use of trade, firm, or product names is for descriptive purposes only and does not imply endorsement by the U.S. Government.

References

Al-Horani, F.A., Al-Moghrabi, S.M., De Beer, D., 2003a. The mechanism of calcification and its relation to photosynthesis and respiration in the scleractinian coral Galaxea fascicularis. Mar. Biol. 142 (3), 419–426.

Al-Horani, F.A., Al-Moghrabi, S.M., de Beer, D., 2003b. Microsensor study of photosynthesis and calcification in the scleractinian coral, Galaxea fascicularis: active internal carbon cycle. J. Exp. Mar. Biol. Ecol. 288 (1), 1–15.

Allison, N., 2017. Reconstructing coral calcification fluid dissolved inorganic carbon chemistry from skeletal boron: an exploration of potential controls on coral aragonite B/Ca. Heliyon 3 (8), e00387.

Allison, N., Finch, A.A., 2010. δ11B, Sr, Mg and B in a modern Porites coral: the relationship between calcification site pH and skeletal chemistry. Geochim. Cosmochim. Acta 74 (6), 1790–1800.

Allison, N., Cohen, I., Finch, A.A., Erez, J., Tudhope, A.W., 2014. Corals concentrate dissolved inorganic carbon to facilitate calcification. Nat. Commun. 5 (1), 1–6.

Andersson, E.R., Stewart, J.A., Work, T.M., Woodley, C.M., Schock, T.B., Day, R.D., 2020. Morphological, elemental, and boron isotopic insights into pathophysiology of diseased coral growth anomalies. Sci. Rep. 10 (1), 1–13.

Baker, D.M., Freeman, C.J., Wong, J.C.Y., Fogel, M.L., Knowlton, N., 2018. Climate change promotes parasitism in a coral symbiosis. ISME J. 12 (3), 921–930.

Balan, E., Pietrucci, F., Gervais, C., Blanchard, M., Schott, J., Gaillardet, J., 2016. First-principles study of boron speciation in calcite and aragonite. Geochim. Cosmochim. Acta 193, 119–131.

Bishop, M., Shahid, N., Yang, J., Barron, A.R., 2004. Determination of the mode and efficacy of the cross-linking of guar by borate using MAS 11B NMR of borate cross-linked guar in combination with solution 11B NMR of model systems. Dalton Trans. 17, 2621–2634.

Burton, E.A., Walter, L.M., 1987. Relative precipitation rates of aragonite and Mg calcite from seawater: temperature or carbonate ion control? Geology 15 (2), 111–114.

Campbell, P.L., Prouty, N.G., Storlazzi, C.D., D'Antonio, N.L., 2017. The Use of Passive Membrane Samplers to Assess Organic Contaminant Inputs at Five Coastal Sites in West Maui. U.S. Geological Survey Open-File Report 2017-1097, Hawaii. https://doi.org/10.3133/ofr20171097, 19 p.

Cochran, S.A., Gibbs, A.E., White, D.J., 2014. Benthic Habitat Map of the U.S. Coral Reef Task Force Watershed Partnership Initiative Kā'Anapali Priority Study Area and the State of Hawai'i Kahekili Herbivore Fisheries Management Area, west-central Maui. U.S. Geological Survey Open-File Report 2014-1129, Hawai'i. https://doi.org/10.3133/ofr20141129, 42 p.

Coles, S.L., Jokiel, P.L., 1977. Effects of temperature on photosynthesis and respiration in hermatypic corals. Mar. Biol. 43 (3), 209–216.

Comeau, S., Tambutté, E., Carpenter, R.C., Edmunds, P.J., Evensen, N.R., Allemand, D., Ferrier-Pagès, C., Tambutté, S., Venn, A.A., 2017. Coral calcifying fluid pH is modulated by seawater carbonate chemistry not solely seawater pH. Proc. R. Soc. B Biol. Sci. 284 (1847), 20161669.

Crain, C.M., Kroeker, K., Halpern, B.S., 2008. Interactive and cumulative effects of multiple human stressors in marine systems. Ecol. Lett. 11 (12), 1304–1315.

Dailer, M.L., Knox, R.S., Smith, J.E., Napier, M., Smith, C.M., 2010. Using $\delta^{15}N$ values in algal tissue to map locations and potential sources of anthropogenic nutrient inputs on the island of Maui, Hawai'i, USA. Mar. Pollut. Bull. 60 (5), 655–671.

Dailer, M.L., Ramey, H.L., Saephan, S., Smith, C.M., 2012. Algal $\delta^{15}N$ values detect a wastewater effluent plume in nearshore and offshore surface waters and three-dimensionally model the plume across a coral reef on Maui, Hawai'i, USA. Mar. Pollut. Bull. 64 (2), 207–213.

DeCarlo, T.M., Holcomb, M., McCulloch, M.T., 2018. Reviews and syntheses: revisiting the boron systematics of aragonite and their application to coral calcification. Biogeosciences 15 (9), 2819–2834.

Dickson, A.G., 1990. Thermodynamics of the dissociation of boric acid in synthetic seawater from 273.15 to 318.15 K. Deep Sea Res. Part A 37 (5), 755–766.

Dickson, A.G., Millero, F.J., 1987. A comparison of the equilibrium constants for the dissociation of carbonic acid in seawater media. Deep Sea Res. Part A 34 (10), 1733–1743.

D'Olivo, J.P., McCulloch, M.T., 2017. Response of coral calcification and calcifying fluid composition to thermally induced bleaching stress. Sci. Rep. 7 (1), 1–15.

Douville, É., Paterne, M., Cabioch, G., Louvat, P., Gaillardet, J., Juillet-Leclerc, A., Ayliffe, L., 2010. Abrupt sea surface pH change at the end of the younger Dryas in the central sub-equatorial Pacific inferred from boron isotope abundance in corals (Porites). Biogeosciences 7 (8), 2445–2459.

Falinski, Kim, Reed, Dana, Callender, Tova, Fielding, Emily, Newbold, Robin, Yurkanin, Alana, 2017. Hui o ka Wai Ola Water Quality Data [Data set]. Zenodo. https://doi.org/10.5281/zenodo.830049.

Farmer, J.R., Branson, O., Uchikawa, J., Penman, D.E., Hönisch, B., Zeebe, R.E., 2019. Boric acid and borate incorporation in inorganic calcite inferred from B/Ca, boron isotopes and surface kinetic modeling. Geochim. Cosmochim. Acta 244, 229–247.

Fietzke, J., Frische, M., 2016. Experimental evaluation of elemental behavior during LA-ICP-MS: influences of plasma conditions and limits of plasma robustness. J. Anal. At. Spectrom. 31 (1), 234–244.

Fietzke, J., Heinemann, A., Taubner, I., Böhm, F., Erez, J., Eisenhauer, A., 2010. Boron isotope ratio determination in carbonates via LA-MC-ICP-MS using soda-lime glass standards as reference material. J. Anal. At. Spectrom. 25 (12), 1953–1957.

Foster, G.L., 2008. Seawater pH, pCO2 and $[CO^{2-}_3]$ variations in the Caribbean Sea over the last 130 kyr: a boron isotope and B/ca study of planktic foraminifera. Earth Planet. Sci. Lett. 271 (1–4), 254–266.

Foster, G.L., Pogge von Strandmann, P.A.E., Rae, J.W.B., 2010. Boron and magnesium isotopic composition of seawater. Geochem. Geophys. Geosyst. 11 (8).

Gagnon, A.C., Gothmann, A.M., Branson, O., Rae, J.W.B., Stewart, J.A., 2021. Controls on boron isotopes in a cold-water coral and the cost of resilience to ocean acidification. Earth Planet. Sci. Lett. 554, 116662.

Giri, S.J., Swart, P.K., Pourmand, A., 2019. The influence of seawater calcium ions on coral calcification mechanisms: constraints from boron and carbon isotopes and B/ca ratios in Pocillopora damicornis. Earth Planet. Sci. Lett. 519, 130–140.

Glenn, C.R., Whittier, R.B., Dailer, M.L., Dulaiova, H., El-Kadi, A.I., Fackrell, J., Kelly, J. L., Waters, C.A., Sevadjian, L., 2013. Lahaina Groundwater Tracer Study – Lahaina, Maui, Hawaii, Final Report. State of Hawaii Department of Health, the U.S. Environmental Protection Agency, and the U.S. Army Engineer Research and Development Center, 502 p.

Gutjahr, M., Bordier, L., Douville, E., Farmer, J., Foster, G.L., Hathorne, E.C., Hönisch, B., Lemarchand, D., Louvat, P., McCulloch, M., Noireaux, J., Pallavicini, N., Rae, J.W.B., Rodushkin, I., Roux, P., Stewart, J.A., Thil, F., You, C.-F., 2021. Sub-Permil Interlaboratory consistency for solution-based boron isotope analyses on marine carbonates. Geostand. Geoanal. Res. 45 (1), 59–75.

Hansen, M.R., Vosegaard, T., Jakobsen, H.J., Skibsted, J., 2004. 11B chemical shift anisotropies in borates from 11B MAS, MQMAS, and single-crystal NMR spectroscopy. J. Phys. Chem. A 108 (4), 586–594.

Hemming, N.G., Hanson, G.N., 1992. Boron isotopic composition and concentration in modern marine carbonates. Geochim. Cosmochim. Acta 56 (1), 537–543.

Hennige, S.J., Wicks, L.C., Kamenos, N.A., Perna, G., Findlay, H.S., Roberts, J.M., 2015. Hidden impacts of ocean acidification to live and dead coral framework. Proc. R. Soc. B Biol. Sci. 282 (1813), 20150990.

Holcomb, M., DeCarlo, T.M., Gaetani, G.A., McCulloch, M., 2016. Factors affecting B/Ca ratios in synthetic aragonite. Chem. Geol. 437, 67–76.

Hughes, A.D., Grottoli, A.G., 2013. Heterotrophic compensation: a possible mechanism for resilience of coral reefs to global warming or a sign of prolonged stress? PLoS One 8 (11), e81172.

Hunt Jr., C.D., Rosa, S.N., 2009. A multitracer approach to detecting wastewater plumes from municipal injection wells in nearshore marine waters at Kihei and Lahaina, Maui, Hawaii. US Geol. Surv. Sci. Investig. Rep. 2009-5253, 166 p.

Kamenos, N.A., Hennige, S.J., 2018. Reconstructing four centuries of temperature-induced coral bleaching on the great barrier reef. Front. Mar. Sci. 5, 283.

Klochko, K., Kaufman, A.J., Yao, W., Byrne, R.H., Tossell, J.A., 2006. Experimental measurement of boron isotope fractionation in seawater. Earth Planet. Sci. Lett. 248 (1–2), 276–285.

Klochko, K., Cody, G.D., Tossell, J.A., Dera, P., Kaufman, A.J., 2009. Re-evaluating boron speciation in biogenic calcite and aragonite using 11B MAS NMR. Geochim. Cosmochim. Acta 73 (7), 1890–1900.

Langdon, C., Atkinson, M.J., 2005. Effect of elevated pCO_2 on photosynthesis and calcification of corals and interactions with seasonal change in temperature/irradiance and nutrient enrichment. J. Geophys. Res. Oceans 110 (C9).

Mason, H.E., Harley, S.J., Maxwell, R.S., Carroll, S.A., 2012. Probing the surface structure of divalent transition metals using surface specific solid-state NMR spectroscopy. Environ. Sci. Technol. 46 (5), 2806–2812.

Mavromatis, V., Montouillout, V., Noireaux, J., Gaillardet, J., Schott, J., 2015. Characterization of boron incorporation and speciation in calcite and aragonite from co-precipitation experiments under controlled pH, temperature and precipitation rate. Geochim. Cosmochim. Acta 150, 299–313.
McConnaughey, T., 1989. ^{13}C and ^{18}O disequilibrium in biological carbonates: I. Patterns. Geochim. Cosmochim. Acta 53, 151–162.
McConnaughey, T.A., Burdett, J., Whelan, J.F., Paull, C.K., 1997. Carbon isotopes in biological carbonates: respiration and photosynthesis. Geochim. Cosmochim. Acta 61 (3), 611–622.
McCulloch, M., Falter, J., Trotter, J., Montagna, P., 2012a. Coral resilience to ocean acidification and global warming through pH up-regulation. Nat. Clim. Chang. 2 (8), 623–627.
McCulloch, M., Trotter, J., Montagna, P., Falter, J., Dunbar, R., Freiwald, A., Försterra, G., Correa, M.L., Maier, C., Rüggeberg, A., 2012b. Resilience of cold-water scleractinian corals to ocean acidification: boron isotopic systematics of pH and saturation state up-regulation. Geochim. Cosmochim. Acta 87, 21–34.
McCulloch, M.T., D'Olivo, J.P., Falter, J., Holcomb, M., Trotter, J.A., 2017. Coral calcification in a changing world and the interactive dynamics of pH and DIC upregulation. Nat. Commun. 8 (1), 1–8.
McCulloch, M.T., D'Olivo, J.P., Falter, J., Georgiou, L., Holcomb, M., Montagna, P., Trotter, J.A., 2018. Boron isotopic systematics in scleractinian corals and the role of pH up-regulation. Boron Isotopes 145–162. Springer.
Mehrbach, C., Culberson, C.H., Hawley, J.E., Pytkowicx, R.M., 1973. Measurement of the apparent dissociation constants of carbonic acid in seawater at atmospheric pressure. Limnol. Oceanogr. 18 (6), 897–907.
Morris, L.A., Voolstra, C.R., Quigley, K.M., Bourne, D.G., Bay, L.K., 2019. Nutrient availability and metabolism affect the stability of coral–Symbiodiniaceae symbioses. Trends Microbiol. 27 (8), 678–689.
Murray, J., Prouty, N.G., Peek, S., Paytan, A., 2019. Coral skeleton $\delta^{15}N$ as a tracer of historic nutrient loading to a coral reef in Maui, Hawaii. Sci. Rep. 9 (1), 5579.
Nalley, E.M., Tuttle, L.J., Barkman, A.L., Conklin, E.E., Wulstein, D.M., Richmond, R.H., Donahue, M.J., 2021. Water quality thresholds for coastal contaminant impacts on corals: a systematic review and meta-analysis. Sci. Total Environ. 794, 148632.
Noireaux, J., Mavromatis, V., Gaillardet, J., Schott, J., Montouillout, V., Louvat, P., Rollion-Bard, C., Neuville, D.R., 2015. Crystallographic control on the boron isotope paleo-pH proxy. Earth Planet. Sci. Lett. 430, 398–407.
Pastorok, R.A., Bilyard, G.R., 1985. Effects of sewage pollution on coral-reef communities. Mar. Ecol. Prog. Ser. 175–189.
Pierrot, D., Lewis, E., Wallace, D.W.R., 2006. MS Excel Program Developed for CO2 System Calculations. http://cdiac.ornl.gov/ftp/co2sys/CO2SYS_calc_XLS/.
Pogoreutz, C., Rädecker, N., Cardenas, A., Gärdes, A., Voolstra, C.R., Wild, C., 2017. Sugar enrichment provides evidence for a role of nitrogen fixation in coral bleaching. Glob. Chang. Biol. 23 (9), 3838–3848.
Porter, J.W., Fitt, W.K., Spero, H.J., Rogers, C.S., White, M.W., 1989. Bleaching in reef corals: physiological and stable isotopic responses. Proc. Natl. Acad. Sci. 86 (23), 9342–9346.
Prouty, N.G., Fietzke, J., 2021. Coral Geochemistry Time Series from Kahekili. U.S. Geological Survey Data Release, West Maui. https://doi.org/10.5066/P9T9WMAK.
Prouty, N.G., Gallagher, C., 2017. Olowalu Chronology and Geochemistry Time-Series. U.S. Geological Survey data release, West Maui. https://doi.org/10.5066/F72J69TH.
Prouty, N.G., Cohen, A., Yates, K.K., Storlazzi, C.D., Swarzenski, P.W., White, D., 2017a. Vulnerability of coral reefs to bioerosion from land-based sources of pollution. J. Geophys. Res. Oceans 122 (12), 9319–9331.
Prouty, N.G., Yates, K.K., Smiley, N.A., Gallagher, C., 2017b. Coral Growth Parameters and Seawater Chemistry, Kahekili. U.S. Geological Survey Data Release, West Maui. https://doi.org/10.5066/F7X34VPV.
Prouty, N.G., Yates, K.K., Smiley, N., Gallagher, C., Cheriton, O., Storlazzi, C.D., 2018. Carbonate system parameters of an algal-dominated Reef along West Maui. Biogeosci. Discuss. 2018, 1–24.
Ries, J.B., Cohen, A.L., McCorkle, D.C., 2009. Marine calcifiers exhibit mixed responses to CO_2-induced ocean acidification. Geology 37 (12), 1131–1134.
Rollion-Bard, C., Blamart, D., Trebosc, J., Tricot, G., Mussi, A., Cuif, J.-P., 2011. Boron isotopes as pH proxy: a new look at boron speciation in deep-sea corals using 11B MAS NMR and EELS. Geochim. Cosmochim. Acta 75 (4), 1003–1012.
Ross, M., White, D., Aiwohi, M., Walton, M., Sudek, M., Lager, D., Jokiel, P., 2012. Characterization of "Dead Zones" and Population Demography of *Porites compressa* along a Gradient of Anthropogenic Nutrient Input at Kahekili Beach Park, Maui. Final Report for Project C11722. State of Hawaii, Department of Land and Natural Resources, Division of Aquatic Resources, Honolulu, Hawaii 96813.
Rosset, S., Wiedenmann, J., Reed, A.J., D'Angelo, C., 2017. Phosphate deficiency promotes coral bleaching and is reflected by the ultrastructure of symbiotic dinoflagellates. Mar. Pollut. Bull. 118 (1–2), 180–187.
Schoepf, V., Jury, C.P., Toonen, R.J., McCulloch, M.T., 2017. Coral calcification mechanisms facilitate adaptive responses to ocean acidification. Proc. R. Soc. B Biol. Sci. 284 (1868), 20172117.
Sen, S., Stebbins, J.F., Hemming, N.G., Ghosh, B., 1994. Coordination environments of B impurities in calcite and aragonite polymorphs: a 11B MAS NMR study. Am. Mineral. 79 (9–10), 819–825.
Sevilgen, D.S., Venn, A., Hu, M., Tambutté, E., de Beer, D., Planas-Bielsa, V., Tambutté, S., 2019. Full in vivo characterization of carbonate chemistry at the site of calcification in corals. Science. Advances 5 (1), eaau7447.
Smith, S.V., Kimmerer, W.J., Laws, E.A., Brock, R.E., Walsh, T.W., 1981. Kaneohe Bay sewage diversion experiment: perspectives on ecosystem responses to nutritional perturbation. Pac. Sci. 35 (4), 279–395.
Smith, J.E., Runcie, J.W., Smith, C.M., 2005. Characterization of a large-scale ephemeral bloom of the green alga Cladophora sericea on the coral reefs of West Maui, Hawaii. Mar. Ecol. Prog. Ser. 302, 77–91.
Stewart, J.A., Christopher, S.J., Kucklick, J.R., Bordier, L., Chalk, T.B., Dapoigny, A., Douville, E., Foster, G.L., Gray, W.R., Greenop, R., 2021. NIST RM 8301 boron isotopes in marine carbonate (simulated coral and foraminifera solutions): inter-laboratory $\delta^{11}B$ and trace element ratio value assignment. Geostand. Geoanal. Res. 45 (1), 77–96.
Storlazzi, C.D., Reguero, B.G., Cole, A.D., Lowe, E., Shope, J.B., Gibbs, A.E., Nickel, B.A., McCall, R.T., van Dongeren, A.R., Beck, M.W., 2019. Rigorously Valuing the Role of US Coral Reefs in Coastal Hazard Risk Reduction. 2331-1258. US Geological Survey.
Swart, P.K., 1983. Carbon and oxygen isotope fractionation in scleractinian corals: a review. Earth Sci. Rev. 19 (1), 51–80.
Swarzenski, P.W., Dulai, H., Kroeger, K.D., Smith, C.G., Dimova, N., Storlazzi, C.D., Prouty, N.G., Gingerich, S.B., Glenn, C.R., 2017. Observations of nearshore groundwater discharge: Kahekili Beach park submarine springs, Maui, Hawaii. J. Hydrol. 11, 147–165.
Thompson, D., McCulloch, M., Cole, J.E., Reed, E.V., D'Olivo, J.P., Dyez, K., Lofverstrom, M., Lough, J., Cantin, N., Tudhope, A.W., 2022. Marginal reefs under stress: physiological limits render Galápagos corals susceptible to ocean acidification and thermal stress. AGU Adv. 3 (1), e2021AV000509.
Trotter, J., Montagna, P., McCulloch, M., Silenzi, S., Reynaud, S., Mortimer, G., Martin, S., Ferrier-Pagès, C., Gattuso, J.-P., Rodolfo-Metalpa, R., 2011. Quantifying the pH 'vital effect'in the temperate zooxanthellate coral Cladocora caespitosa: validation of the boron seawater pH proxy. Earth Planet. Sci. Lett. 303 (3–4), 163–173.
Turner, G.L., Smith, K.A., Kirkpatrick, R.J., Oldfield, E., 1986. Boron-11 nuclear magnetic resonance spectroscopic study of borate and borosilicate minerals and a borosilicate glass. J. Magn. Reson. 67, 544–550.
Vega Thurber, R.L., Burkepile, D.E., Fuchs, C., Shantz, A.A., McMinds, R., Zaneveld, J.R., 2014. Chronic nutrient enrichment increases prevalence and severity of coral disease and bleaching. Glob. Chang. Biol. 20 (2), 544–554.
Venn, A., Tambutté, E., Holcomb, M., Allemand, D., Tambutté, S., 2011. Live tissue imaging shows reef corals elevate pH under their calcifying tissue relative to seawater. PLoS One 6 (5), e20013.
Venn, A.A., Tambutté, E., Holcomb, M., Laurent, J., Allemand, D., Tambutté, S., 2013. Impact of seawater acidification on pH at the tissue–skeleton interface and calcification in reef corals. Proc. Natl. Acad. Sci. 110 (5), 1634–1639.
Wall, M., Fietzke, J., Schmidt, G.M., Fink, A., Hofmann, L.C., De Beer, D., Fabricius, K.E., 2016. Internal pH regulation facilitates in situ long-term acclimation of massive corals to end-of-century carbon dioxide conditions. Sci. Rep. 6 (1), 1–7.
Wall, M., Fietzke, J., Crook, E.D., Paytan, A., 2019a. Using B isotopes and B/ca in corals from low saturation springs to constrain calcification mechanisms. Nat. Commun. 10 (1), 1–9.
Wall, M., Prada, F., Fietzke, J., Caroselli, E., Dubinsky, Z., Brizi, L., Fantazzini, P., Franzellitti, S., Mass, T., Montagna, P., 2019b. Linking internal carbonate chemistry regulation and calcification in corals growing at a Mediterranean CO2 vent. Front. Mar. Sci. 6, 699.
Wiltse, W., 1996. Algal Blooms: Progress Report on Scientific Research. West Maui Watershed.
Woodhead, A.J., Hicks, C.C., Norström, A.V., Williams, G.J., Graham, N.A.J., 2019. Coral reef ecosystem services in the Anthropocene. Funct. Ecol. 33 (6), 1023–1034.
Zeebe, R.E., Wolf-Gladrow, D., 2001. CO_2 in Seawater: Equilibrium, Kinetics, Isotopes. Gulf Professional Publishing.